Theoretical analysis of the non-reciprocal phase shift due to birefringence and topology in fiber ring interferometers

Junhao Liu[a,*], Tianhua Xu[b,c,*]

[a] Department of Fiber-Optic Technology, Tianjin Institute of Electronic Materials, Tianjin, 300220, China
[b] School of Engineering, University of Warwick, Coventry CV4 7AL, United Kingdom
[c] School of Precision Instruments and Opto-Electronics Engineering, Tianjin University, Tianjin, 300072, China

HIGHLIGHTS

- Correct Jones matrix of the fiber coil for backward propagation was given.
- Non-reciprocal phase shift induced by the linear and circular birefringence of the coiled fiber were derived.
- Performance of Fiber-optic gyroscope strongly limited by the intrinsic linear and induced circular birefringence of the coiled fiber.

ARTICLE INFO

Keywords:
Bias error
Fiber-optic gyroscope
Jones Matrix
Reciprocity

ABSTRACT

The non-reciprocal phase shift in fiber ring interferometers due to the fiber birefringence and the path topology is investigated for the first time. It is shown that the resultant birefringence of the fiber, which is the combination of the linear birefringence intrinsic to the fiber and the circular birefringence induced by the twisting in the fiber coiling, is not reciprocal for both rays in the bidirectional propagation due to the path topology confined by the coiled fiber. Our model indicates that the performance of fiber ring interferometers periodically depends on both the linear and the circular birefringence of the coiled fiber, and the bias error can be reduced in the typical fabrication process of the fiber coil.

1. INTRODUCTION

Fiber ring interferometers (FRIs) have wide applications in refractive index sensors [1], temperature sensors [2], fiber loop mirrors [3], optical current transformers [4], and especially fiber-optic gyroscopes [5]. In order to improve the performance of FRIs, research works were dedicated to mitigating two types of error sources from perturbations [6]. One is the intrinsic perturbations such as polarization cross-couplings in fibers [7,8] and splicing misalignments between fibers [9,10]. The other is the external perturbations from surrounding environments such as thermal fields [11-13], magnetic fields [14-16], and thermal stress fields [17-19]. Another new type of error source identified recently is the topology of the optical circuit formed in the coiled fiber [20-24]. Most reported investigations were based on the conviction that optical fibers with the linear birefringence, in the absence of magnetic fields, are reciprocal for bidirectional propagations of the forward light in counter-clockwise (CCW) sense and the backward light in clockwise (CW) sense [25]. This enables Sagnac and Faraday effects to be the only detectable non-reciprocal effects [26]. It concludes that the Jones matrices of the fiber for both rays are mutually transposed [27,28], which have been widely accepted in FRIs [10,14,15]. Unfortunately, it is not true for practical FRIs, where the coiled polarization-maintaining fibers (PMFs) have both linear and circular birefringence. The linear birefringence arises from the thermal stress established in the fiber fabrication, and this is intrinsic to PMFs [29]. The circular birefringence originates from two factors, the internal rotation (IR) of the linear birefringence axes and the external twist (ET) of the fiber. The IR is also intrinsic to the fiber and is established in the drawing process during the fiber fabrication [30,31]. The ET is inevitable in the fiber handlings, such as fiber coiling and splicing [32-34]. Consequently, as shown later in this paper, the resultant elliptical birefringence, which is the combination of the linear and the circular birefringence, is non-reciprocal for bidirectional propagations of light waves in FRIs, although both purely linear and circular birefringence are reciprocal indeed [35-38]. For the first time to our knowledge, it is demonstrated that the Jones matrix (JM) of the coiled fiber for the backward light propagation should be the transpose of that for the

* Corresponding author at: Department of Fiber-Optic Technology, Tianjin Institute of Electronic Materials, Tianjin 300220, China.
E-mail addresses: uxeeux@ucl.ac.uk (J. Liu), tianhua.xu@ieee.org (T. Xu).

https://coi.org/10.1010/j.optlastec.2021.101010
Received 2021;
Available online
1010-1010/

forward light propagation, while with opposite signs for all off-diagonal elements. This relationship works for both light propagations in CCW and CW directions in the fiber coils of FRIs. Therefore, FRIs are non-reciprocal for bidirectional propagations. Both the linear and the circular birefringence of the coiled fiber will produce non-reciprocal errors, which will play important roles in FRIs.

2. THEORY

The optical circuit formed in the coiled fiber of an ideal FRI is illustrated in Fig.1. There is a loop produced in the coiled fiber, which is a circle centered at O with a radius of R. The normal vector to the disk (circle) coincides with the $\hat{x}$-axis of the rectangular coordinate system $\hat{x}\hat{y}\hat{z}$, in which all light beam vectors of this paper are described. The incident light (denoted by an electric vector $\mathbf{E}_0$) is linearly polarized along the $\hat{x}$-axis and travels in the $\hat{z}$-axis direction. The propagation of the light refers to the travel of the electric and magnetic field vectors. For simplicity, only coordinates associated to electric field vectors are listed in Fig. 1. For the light traveling from point O_1 to point O_2 in the CW direction along the arc O_1O_2, it is transferred from the coordinate $x_1y_1z_1$ to the coordinate $x_2y_2z_2$. If the light is propagated along the straight line $\overline{O_1O_2}$, it will be transferred from the coordinate $x_1y_1z_1$ to the coordinate $x_1'y_1'z_1'$. It is obviously found that there is a rotation angle ϑ_2 about the subnormal ($\hat{x}$-axis) introduced during the light propagation along the curved path O_1O_2 and the straight path $\overline{O_1O_2}$. The rotation angle ϑ_2 equals the central angle ϑ_1 subtended by the curved path (arc O_1O_2). That indicates that there is a rotation operation about the subnormal ($\hat{x}$-axis here) when the light travels via the curved path, i.e., the coiled fiber in the FRI. The operation is denoted by the rotation matrix $\mathbf{R}_x(\vec{\vartheta}_x)$ about $\hat{x}$-axis in the CW case, where the left arrow on top of ϑ_x refers to the CW light. Similarly, we have $\vartheta_4 = \vartheta_3$ from the operation of the rotation matrix $\mathbf{R}_x(\vec{\vartheta}_x)$ for the CCW light (denoted by the right arrow). Then we will have

$$\vec{\mathbf{E}} = \mathbf{R}_x(\vec{\vartheta}_x)\mathbf{E}_0 \tag{1a}$$

for the CCW light and

$$\overleftarrow{\mathbf{E}} = \mathbf{R}_x(\overleftarrow{\vartheta}_x)\mathbf{E}_0 \tag{1b}$$

for the CW light propagation in the ideal FRI (no birefringence), respectively. Where the rotation matrix

$$\mathbf{R}_x(\vartheta_x) = \begin{pmatrix} 1 & 0 & 0 \\ 0 & \cos\vartheta_x & \sin\vartheta_x \\ 0 & -\sin\vartheta_x & \cos\vartheta_x \end{pmatrix} \tag{2}$$

describes the impact from the topology of the curved light path formed in the coiled fiber. The rotation angle is named as the phase angle of the topological or geometric phase [15], the anholonomy [16], or the Berry phase [17]. Its value is positive ($\vec{\vartheta}_x > 0$) for the right-handed propagation (CCW light), and is negative ($\vec{\vartheta}_x < 0$) for the left-handed propagation (CW light), since all coordinate systems for describing light travels are right-handed, the same as the initial coordinate system $\hat{x}\hat{y}\hat{z}$.

For the entire loop shown in Fig.1, we have $\vec{\vartheta}_x = 2\pi$ and $\vec{\vartheta}_x = -2\pi$ for the CCW and the CW light propagations, respectively. Then we have $\mathbf{R}_x(\vec{\vartheta}_x) = \mathbf{R}_x(\overleftarrow{\vartheta}_x) = \mathbf{I}$ and hence $\vec{\mathbf{E}} = \overleftarrow{\mathbf{E}}$, where $\mathbf{I}$ denotes the unit matrix. This indicates that the reciprocity works in the coiled fiber when there is no birefringence.

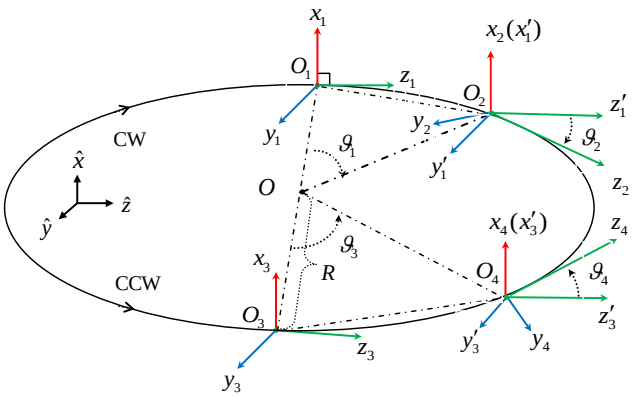

Fig.1. Topological phases introduced by the parallel transport of the light vector traveling along the circular path in the coiled fiber of an ideal FRI. The phase angles are positive for right-handed paths (CCW light) and are negative for left-handed paths (CW light).

In general, a rotation matrix represents the JM of a circular retarder in the optical system [35], to show the polarization rotation (PR) of a linear polarization induced by the circular birefringence of the fiber [36] or the parallel transport of the polarization in the light propagation [24]. The topological phase ϑ_x, from the rotation about $\hat{x}$-axis $\mathbf{R}_x(\vartheta_x)$, can be considered as the retardation effect from an equivalent circular retarder. Similarly, the retardation due to the circular birefringence in a practical fiber can also be regarded as the topological phase ϑ_z from the rotation $\mathbf{R}_z(\vartheta_z)$ about $\hat{z}$-axis. The rotation arises from the IR of the linear birefringence axis and the ET over the PMFs. However, since the parallel transport follows the direction of the rotation axis in this case, the trajectory experienced by the optical vector is a spatial helix as shown in Fig.2, instead of the plane curve in Fig.1. The helix has a fixed handedness. Then topological phase angle ϑ_z is always the same for the forward (traveling from left to right) and the backward (from right to left) rays in Fig. 2. The forward and the backward propagated rays in Fig. 2 refer to the CW and the CCW rays in Fig.1, respectively, with $\hat{z}$-axis in Fig. 2 (the propagation direction of both rays) bended into a loop. Then we have $\vec{\mathbf{E}} = \mathbf{R}_x(\vec{\vartheta}_x)\mathbf{R}_z(\vartheta_z)\mathbf{E}_0$ and $\overleftarrow{\mathbf{E}} = \mathbf{R}_x(\overleftarrow{\vartheta}_x)\mathbf{R}_z(\vartheta_z)\mathbf{E}_0$, i.e., $\vec{\mathbf{E}} = \overleftarrow{\mathbf{E}}$. Therefore, the reciprocity also works in the coiled fiber with the circular birefringence. If we assume fixed rates of τ and ξ (both in rad/m) in the IR and the ET of the fiber with a length of L, the rotation angle ϑ_z about $\hat{z}$-axis is the same for both directions with

$$\vartheta_z = \left[\tau + (1+g)\xi\right]L \tag{3}$$

where $g=-n^2 p_{44}$, n and p_{44} are the refractive index and the Pockels' coefficient, respectively. For the PR introduced by IR and ET showed in equation (3), Jones matrices are same one for CCW and CW lights. The effect from IR and ET of the coiled fiber both for CCW and CW lights, is the same rotation operation about $\hat{z}$-axis, $\mathbf{R}_z(\vartheta_z)$,

$$\mathbf{R}_z(\vartheta_z)=\begin{pmatrix}\cos\vartheta_z & \sin\vartheta_z & 0\\ -\sin\vartheta_z & \cos\vartheta_z & 0\\ 0 & 0 & 1\end{pmatrix}. \tag{4}$$

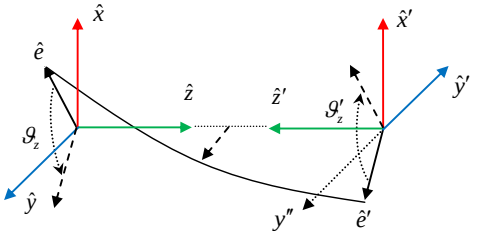

Fig.2. Rotation about the direction of light propagation is a space helix with constant handedness. The rotation angles are same (instead of opposite) for both rays.

It is now found that the reciprocity is held in the coiled fiber when there is no linear birefringence, i.e., purely circular birefringence, as shown in our above analyses. Unfortunately, this will not be applicable in coiled fibers with both the linear and the circular birefringence, i.e., real fiber with the elliptical birefringence. The effect of the linear birefringence can be described using the matrix of a linear retarder $\mathbf{U}=e^{i\bar{\beta}L}\mathrm{diag}[e^{i\Delta\beta L},\ e^{-i\Delta\beta L},\ 1]$, where $\Delta\beta=(\beta_x-\beta_y)/2$ and $\bar{\beta}=(\beta_x+\beta_y)/2$ are halves of the difference between propagation constants and the sum of propagation constants, respectively, and β_x and β_y are propagation constants of the slow-mode and the fast-mode, respectively [36]. Then JMs of the coiled fiber can be written as $\bar{\mathbf{M}}(L)=\mathbf{R}_z(\vartheta_z)\mathbf{U}$ for the CCW light, and $\bar{\mathbf{M}}(L)=\mathbf{U}\mathbf{R}_z(\vartheta_z)$ for the CW light. Note that the orders of the linear and the circular retarders will not affect the unidirectional propagation in the fiber, but they will influence bidirectional propagations, which happen in the coiled fiber of the FRI. This results in the fundamental non-reciprocity in the FRI. Meanwhile, the JMs of the splitter for the reflection and the transmission can be described as $\mathbf{S}_r=\mathbf{R}_x(\pi)\mathbf{S}$ and $\mathbf{S}_t=\mathbf{R}_x(0)\mathbf{S}$ ($\mathbf{S}=\mathbf{I}/\sqrt{2}$), respectively. Then the JMs of the FRI, $\bar{\mathbf{M}}=\mathbf{S}_r\mathbf{R}_x(\vartheta_x)\bar{\mathbf{M}}(L)\mathbf{S}_t$ and $\bar{\mathbf{M}}=\mathbf{S}_t\mathbf{R}_x(\vartheta_x)\bar{\mathbf{M}}(L)\mathbf{S}_r$ can be expressed as

$$\bar{\mathbf{M}}=\frac{e^{i\bar{\beta}L}}{2}\begin{pmatrix}A & B^* & 0\\ B & -A^* & 0\\ 0 & 0 & -1\end{pmatrix} \tag{5a}$$

for the CCW propagation, and

$$\bar{\mathbf{M}}=\frac{e^{i\bar{\beta}L}}{2}\begin{pmatrix}A & -B & 0\\ -B^* & -A^* & 0\\ 0 & 0 & -1\end{pmatrix} \tag{5b}$$

for the CW propagation, where $A=e^{i\Delta\beta L}\cos\vartheta_z$ and $B=e^{i\Delta\beta L}\sin\vartheta_z$. The element -1 indicates the reverse of the propagation direction for the CCW and the CW rays. The relationship between Eq. (5a) and Eq. (5b) has not been correctly clarified in previous works. It was wrongly stated as either the "identity" [25] or the "transposition" [10,14-16]. In fact, JMs of an FRI for the CCW and the CW propagations are mutually transposed with opposite signs for all off-diagonal elements, as for the case of a purely circular retarder [22].

Once correct JMs of the FRI are obtained, the non-reciprocity can be calculated based on following steps [10]. Firstly, the output electric field of the FRI can be written as $\mathbf{E}=\bar{\mathbf{E}}e^{i\varphi/2}+\bar{\mathbf{E}}e^{-i\varphi/2}$, where φ is the Sagnac phase shift. Secondly, the coherence matrix $\mathbf{J}=\mathbf{E}\mathbf{E}^{\dagger}$ of the output electric field can be calculated via the matrix product of the field $\mathbf{E}$ and its Hermitian matrix $\mathbf{E}^{\dagger}$. Thirdly, the trace of the coherence matrix, $\mathrm{tr}\mathbf{J}$, can be acquired through the measured intensity in an optical detector. Fourthly, the null shift φ_0 can be assessed from the condition $\mathrm{d}(\mathrm{tr}\mathbf{J})/\mathrm{d}\varphi|_{\varphi=0}=0$. In the approximation of the plane wave, the null shift φ_0 in the FRI is finally expressed as:

$$\varphi_0=\frac{1}{2}\arctan\frac{2\left[\sin\left(2\Delta\beta L\right)\sin^2\vartheta_z\right]\cdot\left\{\cos^2\vartheta_z-\left[\cos\left(2\Delta\beta L\right)+4\varepsilon\sin^2\left(\Delta\beta L\right)\right]\sin^2\vartheta_z\right\}}{\left[\sin\left(2\Delta\beta L\right)\sin^2\vartheta_z\right]^2-\left\{\cos^2\vartheta_z-\left[\cos\left(2\Delta\beta L\right)+4\varepsilon\sin^2\left(\Delta\beta L\right)\right]\sin^2\vartheta_z\right\}^2}. \tag{6}$$

Equation (6) provides the expression of the null shift φ_0 due to the non-reciprocity of the FRI, with respect to parameters of $\Delta\beta$ and ϑ_z from the linear and the circular birefringence of the fiber, respectively. The FRI is reciprocal, i.e., $\varphi_0=0$, when there is no linear or circular birefringence in the fiber, i.e., $\Delta\beta=0$ or $\vartheta_z=0$, corresponding to an ideal FRI. The non-reciprocity originates from the non-zero linear and circular birefringence in practical fibers and coiling processes in practical FRIs. This indicates the importance of the fiber birefringence. The non-reciprocity described by the null shift in Eq. (6) will vary periodically due to the trigonometric functions of the fiber birefringence. Similar impacts from the polarizer amplitude extinction ratio ε and the fiber length L are also explicitly described in Eq. (6). The same dependence on the fiber birefringence occurs to the bias error of the FRI, since it scales linearly with the null shift via $\Omega_0=K\varphi_0$ according to Sagnac effect, where the scale factor $K=\lambda c/2\pi LD$ is a coefficient dominated by the wavelength λ and the velocity

c of the light in vacuum, as well as the length L and the diameter D of the coiled fiber. It is found that the dependence of the bias error on the fiber birefringence behaves similarly as the null shift does in Eq. (6).

3. CALCULATIONS

Numerical calculations of bias errors are carried out for an FRI according to Eq. (6) and the Sagnac formula, using MATLAB. Parameters are listed in Table 1. The wavelength and the velocity of the light in vacuum are $\lambda = 1{,}550$ nm and $c = 299{,}792{,}458$ m/s, respectively. The average refractive index of the core is $n = \lambda\bar{\beta}/2\pi = 1.4578$. The beat length (indicating the linear birefringence) of the fiber is around $\Lambda = \pi/\Delta\beta = 3.0$ mm. The circular birefringence of the fiber manifests itself as the induced PR. The total length of the fiber is $L = 1000$ m. The amplitude extinction ratio of the polarizer is $\varepsilon = E_{0y}/E_{0x} = 0.1$. It is clearly found that the bias errors show periodical dependence on the linear and the circular birefringence of the fiber, as results in Fig. 3 and Fig. 4. The performance fluctuation of practical FRIs can be explained based on such dependence. The bias errors can span several orders of magnitude, even for the same batch of FRIs. It ranges from the best case (0 deg/h for both the linear and the circular birefringence) to the worst case (± 0.24 deg/h for the circular birefringence and ± 0.024 deg/h for the linear birefringence). It can also be found from Eq. (6) that the circular birefringence of the fiber plays a more dominant role for the performance of FRIs.

Table 1

Parameters used in numerical simulations.

Symbol	Parameter	Value	Reference
c	Speed of light in vacuum	299,792,458 m/s	[5,6]
λ	Wavelength in vacuum	1,550 nm	
n	Refractive index of fiber	1.4578	[29]
Λ	Beat length of fiber	3.0 mm	[29,31]
L	Fiber length	1,000 m	[13]
D	Diameter of fiber loop	100 mm	[13]
p_{44}	Pockels coefficient	-0.075	[33]
ξ	External twist rate of the PMFs	0.01-0.1 deg/mm	[32-34]
ε	Amplitude extinction ratio of the polarizer	0.1	[10]
τ	Internal rotation rate of the linear birefringence axes of the PMFs	0.01-0.5 deg/mm	[30,31]

The periodic dependence of bias errors on the PR induced by the circular birefringence of the fiber is shown in Fig. 3(a). Within each period, there is a clear discontinuity point between the upper and the lower halves. Singularities are located at the middle and the edges of each period, corresponding to the worst bias errors of the FRI, which gives $\pm\Omega_{0\max} = \pm 0.24$ deg/h with $\mathrm{PR} = \vartheta_z \approx 58$ deg/h in the example here. The worst null shift is $\varphi_{0\max} = (1/2)\arctan[-(\tan 2\vartheta_z)/2]$ accordingly, where PR is given by $\vartheta_z = \operatorname{arccot}\{\pm[4\varepsilon\sin^2(\Delta\beta L) + \cos(2\Delta\beta L) + \sin(2\Delta\beta L)]^{1/2}\}$. This will occur at angles of $\vartheta_z = \pm(2k+1)\pi/4$ ($k = 0,1,2,3\cdots$) when the following two conditions are satisfied. One is that the polarizer should be ideal, i.e., $\varepsilon = 0$, and the other is that the fiber length should be the odd multiples of a quarter of the beat length, i.e., $L = (2k+1)\Lambda/4$. The two conditions arise from $\cos(2\Delta\beta L) = 0$ and the two opposite maxima come from $\sin(2\Delta\beta L) = \pm 1$.

There are two different minima, at the middle of the upper and the lower halves within a period, respectively. The first minimum i.e., the optimal bias error $\Omega_{0\mathrm{opt}} = 0$ (corresponding to $\varphi_{0\mathrm{opt}} = 0$), always occurs at $\vartheta_z = \pm k\pi$ in the lower half. It means that the total PR vanishes (equal to 0 or integral multiples of π for the linear polarization). This shows the condition to achieve the best performance of an FRI, which is independent of the linear birefringence in the fiber. The second minimum $\Omega_{0\min}$ is located at the middle of the upper half. At this position, the PR induced by the circular birefringence is given by $\vartheta_z = \pm(2k+1)\pi/2$. This means that the polarization of the output light is orthogonal to the polarization of the incident light. The general expression of the null shift for this second minimum can be attained by substituting the conditions of $\sin\vartheta_z = \pm 1$ and $\cos\vartheta_z = 0$ into corresponding terms in Eq. (3). The second minimum is always positive and larger than the first minimum, i.e., $\Omega_{0\min} > \Omega_{0\mathrm{opt}} = 0$. We will have $\varphi_{0\min} = 2\Delta\beta L$ in the case of an ideal polarizer ($\varepsilon = 0$), and here we have $\Omega_{0\min} = K\varphi_{0\min} = 0.15$ deg/h in our example.

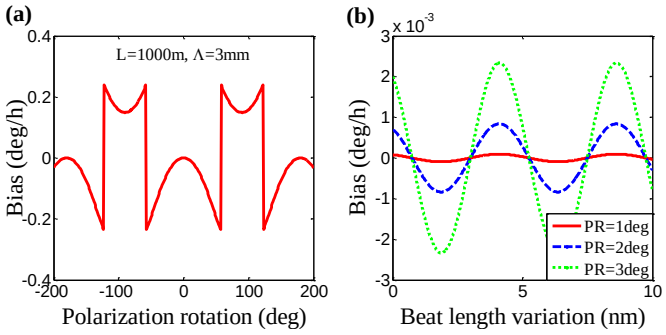

Fig.3. Dependence of bias errors on (a) the PR induced by the circular birefringence and (b) the beat length variation of the coiled fiber in a FRI.

The periodic dependence of bias errors on the linear birefringence of fibers in FRIs is shown in Fig. 3(b). Three curves provide bias values as functions of variations in beat length, $\Delta\Lambda = \Lambda^2/2L$. It is found that the considered beat length varies in the level of nanometer, which is very small to adjust in practical fibers. In our example in Fig. 3(b), we have $\Lambda = 3.00$ mm, and the variation of bias errors ranges from 0 nm to 10 nm. The fluctuations of bias errors span several orders of magnitude for a non-zero PR. They range from the optimal value of 0 deg/h to the worst cases of $\pm 0.1\times 10^{-3}$ deg/h, $\pm 0.8\times 10^{-3}$ deg/h, and $\pm 2.4\times 10^{-3}$ deg/h for PRs of 1 deg, 3 deg, and 5 deg, respectively. The periods of three schemes are all $\Delta\Lambda = 4.5$ nm. Such a small period, at nanometer level, indicates the extremely high and

sensitive dependence of bias errors on the linear birefringence. It arises from the zero linear birefringence term in Eq. (6), $\cos(2\Delta\beta L)=0$, i.e., $\cos(2\Delta\beta L)=\cos(2\pi L/\Lambda)=0$. The high dependence of bias errors on the fiber length can also be observed, as shown in Fig. 4(a), for the same three PR values. The periods for all three PRs equal the beat length. The optimal bias error $\Omega_{0opt}=0$ always occurs when the PR vanishes. For $PR\neq 0$, the optimal bias $\Omega_{0opt}=0$ occurs at the integral multiples of half the beat length, i.e., $L=k\Lambda/2$, according to the condition of $\sin(2\Delta\beta L)=0$. The worst bias errors take place at the odd multiples of a quarter of the beat length.

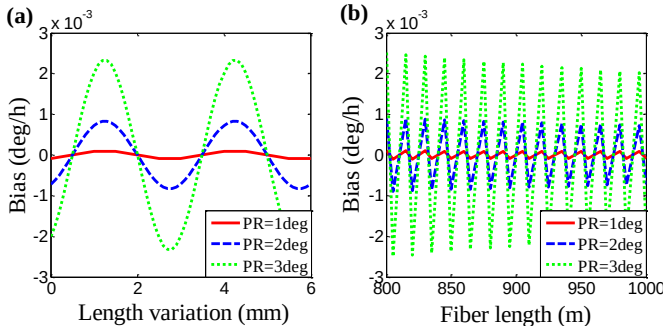

Fig.4. Dependence of bias errors on (a) length variation induced by fiber end cutting at the level of millimeter and (b) total length of the coiled fiber in a FRI.

The dependence of bias errors on the total length of the fiber is shown in Fig. 4(b). The period (equal to the beat length) is still at the level of millimeter, similar as in Fig. 4(a). It is observed in Fig. 4(b) that the amplitudes of maxima decrease with the increment of fiber lengths. It indicates that Sagnac effect is enhanced in FRIs with the increase of fiber lengths. This property also works in results in Fig. 3(b) and Fig. 4(a), but is more clearly observed in Fig. 4(b). This means that the performance improvement by increasing the fiber length is not so obvious for FRIs, especially when the fiber length varies within the same order of magnitude. On the contrary, the dependence on the birefringence is much more significant, and can be applied to efficiently improve the performance of FRIs. The performance improvement originates from the periodic dependence of the null shift in Eq. (6) or bias errors in Fig. 3 and Fig. 4. This can be controlled via the fiber splicing, a typical process in the assembly and the manufacture of FRIs to link coiled fibers to polarizers. The length and the birefringence of the fiber can be adjusted by operations e.g., fiber end cutting and facet alignment, in the slicing process, respectively. There are inevitable twists applied to the fiber in the facet alignment, which will introduce a third PR through the same way as the ET. The total PRs will be the sum of all additional PRs and intrinsic PR induced by the circular birefringence of the fiber. If the twist PR behaves in an opposite way to the intrinsic PR, the alignment-introduced PR will mitigate the intrinsic PR to some extent. Then the performance will be optimized and maintained around the zero points, as shown in Fig. 3(a). A similar improvement can be realized in the cutting process (via several trials of the precise cutting) according to the length variation shown in Fig. 4(a). Such performance improvement relies on two aspects. One is the uniformity of FRIs fabricated in the same batch, e.g., in the above splicing method. The other is the stable response of FRIs to external (e.g., thermal and magnetic) perturbations, which will be investigated in our future work.

4. CONCLUSION

In summary, the non-reciprocal phase shift in FRIs due to the birefringence and the topology of the coiled fiber is investigated based on the topological phase method. It is found that the performance periodically depends on both the linear and the circular birefringence of the fiber. Such dependence allows significant improvements in the performance via typical operations in the fabrications.

CRediT authorship contribution statement

Junhao Liu: Conceptualization, Methodology, Writing, Software. **Tianhua Xu**: Editing, Project supervision.

Declaration of Competing Interest

The authors declare no conflicts of interest.

Acknowledgement

This work is supported by EU Horizon 2020 MSCA-RISE Grant 101008280.

References

[1] C. Han, H. Ding, X. Li, and S. Dong, Temperature insensitive refractive index sensor based on sing-mode micro-fiber Sagnac loop interferometer, App. Phys. Lett. 104 (2014) 181906.
[2] A. N. Starodumov, L. A. Zenteno, D. Monzon, and E. De La Rosa, Fiber Sagnac interferometer temperature sensor, App. Phys. Lett. 70 (1997) 19-21.
[3] D. Leandro and M. Lopez-Amo, All-PM fiber loop mirror interferometer analysis and simultaneous measurement of temperature and mechanical vibration, J. Lightwave Technol. 36 (2018) 1105-1111.
[4] K. Sasaki, M. Takahashi, and Y. Hirata, Temperature-insensitive Sagnac-type optical current transformer, J. Lightwave Technol. 33 (2015) 2463-2467.
[5] H. C. Lefevre, *The Fiber-Optic Gyroscope*, 2nd ed., Artech House, Boston/London (2014).
[6] G. B. Malykin and V. I. Pozdanyakova, *Ring Interferometry*, Walter de Gruyter GmbH, Berlin/Boston (2013).
[7] R. Luo, Y. Li, S. Deng, C. Peng, and Z. Li, Effective suppression of residual coherent phase error in a dual-polarization fiber optic gyroscope, Opt. Lett. 43 (2018) 815-818.
[8] J. Chamoun and M. J. F. Digonnet, Noise and bias error due to polarization coupling in a fiber optic gyroscope, J. Lightwave Technol. 33 (2015) 2839-2847.
[9] H. Liu, Y. Ma, Y. Long, B. Yan, W. Wang, L. Shan, W. Yu, and P. Li, Fiber splicing process research for high-precision optical path assembly of IFOG, J. Lightwave Technol. 34 (2016) 4343-4353.
[10] S. M. Kozel, V. N. Listvin, S.V. Shatalin, and R. V. Yushkaitis, Effect of random inhomogeneities in a fiber lightguide on the null shift in a ring interferometer, Opt. Spect (USSR). 61 (1986) 814-816.
[11] D. M. Shupe, Thermally induced nonreciprocity in the fiber-optic interferometer, Appl. Opt. 19 (1980) 654-655.
[12] F. Mohr, Thermooptically induced bias drift in fiber optical Sagnac interferometers, J. Lightwave Technol. 14 (1996) 27-41.
[13] J. Liu, Y. Liu, and T. Xu, Bias error and its thermal drift due to fiber birefringence in interferometric fiber-optic gyroscopes, Opt. Fiber Technol. 55 (2020) 102138.
[14] D. Zhang, Y. Zhao, W. Fu, Nonreciprocal phase shift caused by magnetic-thermal coupling of a polarization maintaining fiber optic gyroscope, Opt. Lett. 39 (2014) 1382-1384.

[15] T. Saida and K. Hotate, General formula describing drift of interferometer fiber-optic gyro due to Faraday effect: reduction of the drift in twin-depo-I-FOG, J. Lightwave Technol. 17 (1999) 222-228.
[16] K. Hotate and K. Tabe, Drift of an optical fiber gyroscope caused by the Faraday effect: influence of the earth's magnetic field, App. Opt. 25 (1986) 1086-1092.
[17] S. Ogut, B. Osunluk, and E. Ozbay, Modeling of thermal sensitivity of a fiber optic gyroscope coil with practical quadrupole winding, Proc. SPIE 10208, (2017) 1020806
[18] F. Mohr and F. Schadt, Bias error in fiber optic gyroscopes due to elastooptic interactions in the sensor fibers, Proc. SPIE 5502, (2004) 410.
[19] F. Mohr and F. Schadt, Error signal formation in FOGs through thermal and elastooptical environment influences on the sensing coil, ISS Conference, Karlsruhe, (2011).
[20] M. V. Berry, Interpreting the anholonomy of coiled light, Nature 326 (1997) 277-278.
[21] R. Bhandari, Light propagation through a coiled optical fiber and Pancharatnam phase, J. Opt. Soc. Am. B. 24 (2007) 2343.
[22] R. Bhandari, Transpose symmetry of the Jones matrix and topological phases, Opt. Lett. 33 (2008) 854-856.
[23] A. Tomita and R. Y. Chiao, Phys. Rev. Lett. 57 (1986) 937-940.
[24] E. M. Fins and W. Dultz, Rotation of the polarization plane in optical fibers, J. Lightwave Technol. 15 (1997) 144-147.
[25] G. Schiffner, W. R. Leeb, H. Krammer, and J. Wittmann, Reciprocity of birefringent single-mode fibers for optical gyros, App. Opt. 18 (1979) 2096-2097.
[26] V. A. Lodi and S. Donati, Combined reciprocal and non-reciprocal birefringence in optical monomode fibres, Opt. Quant. Elect. 15 (1983) 381-388.
[27] L. Deak and T. Fulop, Reciprocity in quantum, electromagnetic and other wave scattering, Ann. Phys. 327 (2012) 1050-1077.
[28] M. Mansuripur and D. P. Tsai, New perspective on the reciprocity theorem of classical electrodynamics, Opt. Commun. 284 (2011) 707-714.
[29] J. Liu, Y. Liu, and T. Xu, Analytical estimation of stress-induced birefringence in Panda-type Polarization-maintaining fibers, Photon. Technol. Lett. 32 (2020) 1507-1510.
[30] M. J. Marrone, C. A. Villarruel, N. J. Frigo, and A. Dandridge, Internal rotation of the birefringence axes in polarization-holding fibers, Opt. Lett. 12 (1987) 60-62.
[31] J. Liu, Simple method for determining the internal rotation of birefringence axes in polarization-maintaining optical fibers, Opt. Eng. 54 (2015) 086101.
[32] P. McIntyre and A. W. Snyder, Light propagation in twisted anisotropic media: Application to photoreceptors, J. Opt. Soc. Am. 68 (1978) 149-157.
[33] R. Ulrich and A. Simon, Polarization optics of twisted single-mode fibers, App. Opt. 18 (1979) 2241-2251.
[34] H. J. Khozondar, M. S. Muller, R. J. Khozondar, and A. W. Koch, Polarization rotation in twisted polarization maintaining fibers using a fixed reference frame, J. Lightwave Technol. 27 (2009) 5590-5596.
[35] R. C. Jones, A new calculus for the treatment of optical systems I. description and discussion of the calculus, J. Opt. Soc. Am. 31 (1941) 488-493.
[36] F. P. Kapron, H. F. Borrelli, and D. B. Keck, Birefringence in dielectric optical waveguides, J. Quantum Electron. 8 (1972) 222-225.
[37] M. Martinelli and P. Martelli, Polarization, mirrors, and reciprocity: birefringence and its compensation in optical retracing circuits, Adv. Opt. Photon. 9 (2017) 129-168.
[38] D. Tentori and A. G.-Weidner, Jones birefringence in twisted single-mode optical fibers, Opt. Express 21 (2013) 31725-31739.